Materials Advances

ROYAL SOCIETY OF CHEMISTRY

PAPER

View Article Online
View Journal | View Issue

Cite this: *Mater. Adv.*, 2025, 6, 8635

Deep traps in Ga_2O_3 Schottky diodes induced by soft electric breakdown

Alexander Y. Polyakov,[a] Ivan Shchemerov,[a] Eugene B. Yakimov,[ab] Alexey Chernykh,[a] Sergey Chernykh,[a] Anton Vasilev,[a] Nikolai Matros,[a] Andei Romanov,[a] Luiza Alexanyan,[a] Eugene E. Yakimov[ab] and Stephen J. Pearton *[c]

Received 1st August 2025,
Accepted 16th October 2025

DOI: 10.1039/d5ma00831j

rsc.li/materials-advances

We report the electrical characteristics and deep trap behavior of vertical Ga_2O_3 Schottky diodes with diameters ranging from 200 to 380 μm, fabricated on commercial n/n$^+$ epistructures. There was a significant inverse relationship between diode diameter and breakdown voltage (V_B). Specifically, the V_B for a 200 μm diameter diode was 330 V, decreasing to 225 V for 300 μm, and further to 200 V for 380 μm diameter diodes. This scaling is attributed to pre-existing extended defects and those forming under high voltage stress, which act as localized electric field concentrators and enhance current leakage. Electron beam induced current (EBIC) mapping post-breakdown revealed new bright spots and lines within the diodes, indicative of increased local current gain due to defect agglomerates. Following breakdown, a pronounced increase in reverse current was observed at low voltages, which is explained by Poole–Frenkel hopping. This hopping mechanism is predominantly mediated by deep centers with energy levels near E_c −0.7 eV, identified as the dominant E2* traps from pre-breakdown deep trap spectra. While capacitance deep level transient spectroscopy (DLTS) showed only slight changes in trap concentrations, current deep level transient spectroscopy (CDLTS) exhibited a strong signal for E1 and E2* traps after breakdown, suggesting a non-uniform formation of these centers in the vicinity of extended defects, leading to enhanced localized leakage.

Introduction

The thermodynamically stable polymorph β-Ga_2O_3 is a promising material for next generation power electronic devices because of the commercial availability of high electrical and structural quality, large diameter native substrates grown from the melt.[1,2] In addition, there is a strong experience base with epitaxial films prepared by various techniques, and rapidly maturing processing techniques for fabrication of power devices with impressive performance.[1,2] Currently substrates with up to 6-inch diameter prepared by edge-defined film-fed growth (EFG) or Bridgman techniques are commercially available, while epitaxial films of Ga_2O_3 can be grown by halide vapor phase epitaxy (HVPE), metal organic chemical vapor deposition (MOCVD), molecular beam epitaxy (MBE).[1–10] Crystals and films can be doped n-type with concentrations between 10^{15} cm^{-3} and 10^{19} cm^{-3}, or made semi-insulating with high resistivity by Fe, N or Mg doping.[2] The absence of viable p-type doping in Ga_2O_3 has been circumvented by growth of p–n heterojunctions of n-Ga_2O_3 with naturally p-type wide-bandgap compounds among which the most prominent are heterojunctions (HJs) of p-NiO/n-Ga_2O_3. Efforts to master p-type formation in β-Ga_2O_3 by using complexes of Ga vacancy acceptors with hydrogen or by capitalizing on hopping conductivity *via* deep acceptors have also shown promise.[11] Ohmic and Schottky contact formation, preparation of Metal–Insulator–Semiconductor (MIS) structures, ion implantation and annealing, dry etching and passivation processes are also well advanced.[1–10]

There have been numerous theoretical and experimental studies of defects in Ga_2O_3, their introduction by irradiation and their transformation upon annealing.[12–19] This has aided development of Ga_2O_3-based power devices with promising performance such as power rectifiers with breakdown voltages of about 10 kV[20,21] resistant to high power surges[22] or power Field Effect Transistors (FETs) with breakdown voltages of 10 kV[23] and high-power FETs with oscillation frequencies of 35 GHz.[24]

Breakdown voltage is an important characteristic of power devices. An extensive general treatment of the factors determining the values of breakdown voltage in wide-bandgap

[a] National University of Science and Technology MISiS, Moscow, Leninsky pr. 4, Moscow 119049, Russia
[b] Institute of Microelectronics Technology and High Purity Materials, Russian Academy of Sciences, 6 Academician Ossipyan str., Chernogolovka, Moscow Region 142432, Russia
[c] Department of Materials Science and Engineering, University of Florida, Gainesville, FL 32611, USA. E-mail: spear@mse.ufl.edu

semiconductors including Ga_2O_3[25] underlines the difficulties in achieving robust avalanche breakdown in wide-bandgap semiconductors. Point and extended defects are important in the processes leading to early breakdown *via* the formation of defect leakage paths through extended defects. Deep level defects determining the mechanisms of current flow in high electric fields through changing the charge occupation of defect centers and their possible migration, thus influencing the electric field strength and tunneling probabilities of charge carriers.

Recently multiple experimental papers have treated various aspects of defect transformations as affecting the electric breakdown and current instabilities in Ga_2O_3 devices. The structural changes observed in Ga_2O_3 power Schottky diodes were reported in a number of *ex situ* and *in situ* transmission electron microscopy studies[26–29] that revealed formation of vacancy clusters and amorphized inclusions under electrical stress that could be transformed into dislocations and stacking faults and lead to premature breakdown.

Photoluminescence (PL) studies of trench Ga_2O_3 structures subjected to high electrical stress revealed nanometer-scale movement of defects responsible for 3.2 eV and 3.6 eV PL bands attributed to self-trapped-holes (STH) states formed at two different oxygen atoms sites O1 and O2.[30] This has been attributed to the local difference in the oxygen vacancies formation and movement consequently changing the local relative concentrations of the O1 and O2 sites.

Monitoring of changes caused by prolonged forward bias stress and application of high reverse bias on the shape of current–voltage *I–V* characteristics of NiO/Ga_2O_3 HJ rectifiers at different temperatures[31] showed a shift of the turn-on voltage ΔV_{on} and emergence of shoulders in the forward *I–V* characteristics. Those were accompanied by an increase in reverse current. Both the ΔV_{on} and the reverse current recovered with time after the stress. The stress time was changed from 1 s to 10 000 s at three different temperatures. From the dependence of ΔV_{on} on stress and recovery times, an activation energy of 0.46 eV was deduced and attributed to the operation of electron trap with that energy. Such stress led to a strong decrease of the breakdown voltage from 1.9 kV to 1.2 kV.

In a similar stress test, Sijie Bu *et al.*[32] monitored *I–V* characteristics changes of Ga_2O_3 Schottky diodes induced by forward current stress at 8V for 50 s, 500 s and 5000 s and observed a marked increase in both forward current and reverse current with the emergence of a low voltage step in forward current. Simultaneously, it was observed that the ideality factor in the forward current branch increased from $\eta = 1$ to >4 after stress. Analyzing the temperature dependence of reverse current showed it was described by the Poole–Frenkel[32,33] mechanism assuming hopping of injected electrons *via* deep traps with the activation energy of 0.76 eV. This is very close to the predominant deep electron trap detected in deep level transient spectroscopy (DLTS) measurements ascribed to the so-called E2* electron trap associated with gallium vacancies V_{Ga} or V_{Ga}–V_O divacancies.[34] After the electrical stress, the concentration of this E2* center increased in the region adjacent to the Schottky diode with the current flow determined by the trap-assisted tunneling mechanism.[35]

Alternative explanations of the nature of deep traps determining the changes of electrical properties of NiO/Ga_2O_3 p–n HJs and Ga_2O_3 Schottky diodes have also appeared.[36,37] In the first of these, the decrease of forward current of the HJ and increase of the series resistance has been attributed to the emergence of deep hole traps at E_v + 1.3 eV attributed to a complex of Ga vacancy V_{Ga} acceptors with hydrogen. It was postulated the emergence of this feature is due to increase in V_{Ga} density and the release of free hydrogen available for complexing. In the second paper, a correlation was noted between the decrease of breakdown voltage in Ga_2O_3 Schottky diodes with the difference in density of E3 electron traps near E_c −1.1 eV tentatively associated with oxygen vacancies V_O. This was demonstrated by *I–V* measurements and DLTS spectra measurements performed on Schottky diodes prepared on commercial epitaxial structure that contained the E3 centers only in the ∼180 nm of the sample adjacent to the Schottky diode. The breakdown voltage remarkably increased once this E3-rich layer had been removed by polishing. The forward bias stressing caused reverse breakdown degradation and thermally induced failure on both the Ni/Au Schottky contact and the epitaxial layer due to the low thermal conductivity of Ga_2O_3.[36] The temperature profile at the surface during the rectifier turn-on period showed a strong dependence with crystalline orientation. The maximum junction temperature rise occured at the center of the metal contact and was in the range 270–350 °C. Stabilization of Schottky rectifiers under thermal aging is enhanced by formation of PtOx interfacial layers.[37]

The question of which deep traps in Ga_2O_3 affect or are correlated with breakdown voltage is currently not clear.[38] In this paper, we present electrical breakdown measurements and deep trap analysis performed on Ni Schottky diodes prepared on commercial epistructure of the type now commonly used for fabrication of high-performance power rectifiers. Because no edge termination techniques were used in our structure, the measured breakdown voltages are lower than in more refined devices, but the observations are still relevant to understanding the nature of underlying processes.

Experimental

The vertical Schottky diode rectifiers were prepared on commercial n-Ga_2O_3 (shallow Si donor concentration $N_d = 2 \times 10^{16}$ cm^{-3}) 10-μm-thick epitaxial structures grown by halide vapor phase epitaxy (HVPE) on (001)-oriented 600-μm thick n^+-Ga_2O_3 Sn doped ($N_d = 3 \times 10^{18}$ cm^{-3}) substrates fabricated by edge-defined film-fed (EFG) method (Tamura/Novel Crystal Technologies, Japan). The top epitaxial surface was chemo-mechanically polished and epi-ready, the back substrate surface was mechanically polished. The back full-area Ohmic contact was prepared by deposition of Ti/Au (40 nm/80 nm). A set of Ni/Au (50 nm/350 nm) Schottky diodes with diameters 200, 300 μm or 380 μm was prepared by photolithography.

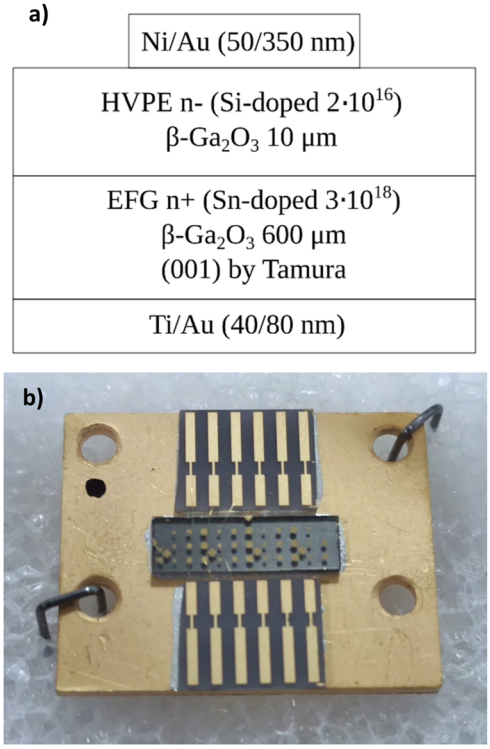

Fig. 1 Ga_2O_3-based Schottky diode. (a) – diode structure, (b) – sample photo.

No mesa etching and passivation was applied in preparation of these structurers. Samples were mounted on the gold-plated Kovar alloy plate with conductive glue. Diodes were wired using thermocompression with 18 μm gold wires. The diode structure and a photograph of the sample are shown in Fig. 1(a and b).

The fabricated diodes were characterized by current–voltage (*I–V*) measurements from 80–500 K using either Agilent B1500 semiconductor parameter analyzer (USA) and Linkam HFSX350-PB4 Probe Stage (Great Britain) or B2902A current–voltage source/meter (Keysight Technologies, USA) and cold-finger liquid nitrogen cryostat (Cryotrade, Russia).[39] Capacitance–voltage (*C–V*) profiling in the frequency range 20 Hz–20 MHz was performed to obtain the charge concentration profiles and the Schottky barrier height *versus* temperature in the temperature range 80–500 K. These measurements were done using either Agilent B1500 semiconductor parameters analyzer (USA) or E4980A LCR meter (Keysight Technologies, USA). These devices were also used to measure the temperature dependence of capacitance and AC conductance at different frequencies (so called Admittance Spectra (AS)[40] and to measure Deep Level Transient Spectra (DLTS).[39,40] Such measurements were complemented by Current Deep Level Transient Spectra[40] using B2902A current–voltage source/meter (Keysight Technologies, USA). Experimental setups are described elsewhere.[41–43] Breakdown voltage (V_B) and high-voltage IV measurements were performed using Keysight B2987B source-meter (Keysight Technologies, USA) at room temperature. When measuring BV, samples were connected to source in series with protection resistor 20 MΩ, so that the current was limited and breakdown was non-destructive (“soft” breakdown). V_B measurements were provided using pulse method: high negative voltage was pulsed from zero bias for 50 ms with 1 s pause between pulses.

In addition, the samples were characterized by electron beam induced current (EBIC) mapping using a scanning electron microscope JSM-840 SEM (JEOL) at room temperature with beam energy E_b varying from 10 keV to 30 keV and beam current of 0.1 nA. A Keithley 428 Keithley, USA) current amplifier was used. The mapping was performed with and without application of reverse bias. The reverse bias was changed from 0 V to −5 V. EBIC images were obtained with dwell time 5 μs per pixel and 1024 × 1024 pixel per frame. The experimental setup is described elsewhere.[44,45]

Results and discussion

Room temperature *I–V* characteristics of diodes as a function of diameter are presented in Fig. 2(a). The reverse current at voltages below 10 V was extremely low and close to the detection limit. At elevated temperatures, the reverse current linearly increased with the ratio of the diode area *S* to diode perimeter *P*, indicating prominent perimeter-related leakage (Fig. 2(c)).[40] The turn-on voltage was about 0.8 V if assessed, as is usual, this value to be corresponding to the current density exceeding 10^{-3} A cm^{-2} (note that Fig. 2(a) presents the current dependence on voltage, not the current density dependence). The specific series resistance at room temperature was 10 mΩ cm^2 and the ideality factor close to 1. The saturation current in forward direction increased with an activation energy of 1.1 eV. The reverse-recovery time from forward current 20 mA was 6 ns.

In *C–V* profiling, the $1/C^2$ *versus* voltage dependences were linear, indicating a uniform shallow donor density distribution for depths up to at least 0.7 μm (Fig. 3(a)). The measured carrier concentration was not dependent on temperature, indicating a low contribution of deep traps, while the built-in voltage was 1 V at room temperature and changed slightly with temperature (Fig. 3(b)).

DLTS spectra measurements revealed the presence of dominant electron traps with level at E_c −0.72 eV, electron capture cross-section $\sigma_n = 2.4 \times 10^{-15}$ cm^2, so called E2* trap often attributed to Ga vacancy–nitrogen vacancy (V_{Ga}–V_O) complexes.[33] Two other centers detected were so called E2 trap near E_c −0.8 eV ($\sigma_n = 2.5 \times 10^{-14}$ cm^2) associated with Fe acceptors on Ga site,[33] and electron trap E1 with level near E_c −0.6 eV ($\sigma_n = 1.4 \times 10^{-14}$ cm^2) assigned to complexes of Si donors with hydrogen.[33] Fig. 4(a) shows the spectra of $\Delta C = C(t_1) - C(t_2)$ normalized by steady-state capacitance *C*, with t_1 and t_2 being the time windows.[40] We did not see a measurable signal from the electron traps E3 with level near E_c −1.1 eV[33] that were reported to be very prominent in some Ga_2O_3 rectifiers and associated with lowering of the observed breakdown voltages in rectifiers.[39] The carrier concentration profiles and the deep traps concentration profiles obtained by measurements

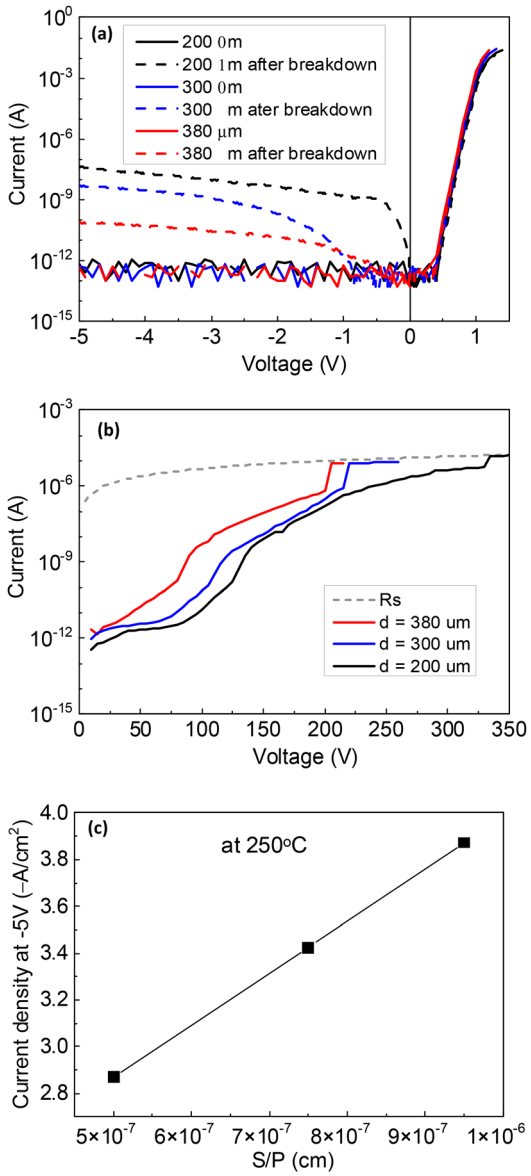

Fig. 2 (a) Room temperature I–V characteristics measured for diode diameters 200, 300 and 380 μm before and after electric breakdown; (b) reverse current voltage characteristics at high voltages for different diode diameters, the dashed line shows the current limited by the 20 MΩ resistor in series; (c) current density at 250 °C at −5 V as a function of the ratio of diodes area S to diodes perimeter P.

with reverse bias voltages up to 30 V (the depth of 1.5 μm) showed that both are fairly uniform.

CDLTS measurements were performed by keeping the sample at reverse bias −40 V and pulsing voltage to 1 V for 1 s. Fig. 4(b) shows the spectra of $\Delta I = I(t_1) - I(t_2)$ normalized to the steady-state current I_{ss} at −40 V. The sensitivity to deep traps of CDLTS is lower than in capacitance DLTS and no measurable spectra could be observed before the breakdown.

Fig. 2(b) presents the results of the "soft" breakdown voltage measurements for the diodes with different diameters. (We here call the breakdown "soft" in the technical sense that the series resistance switched in series with the Schottky diode

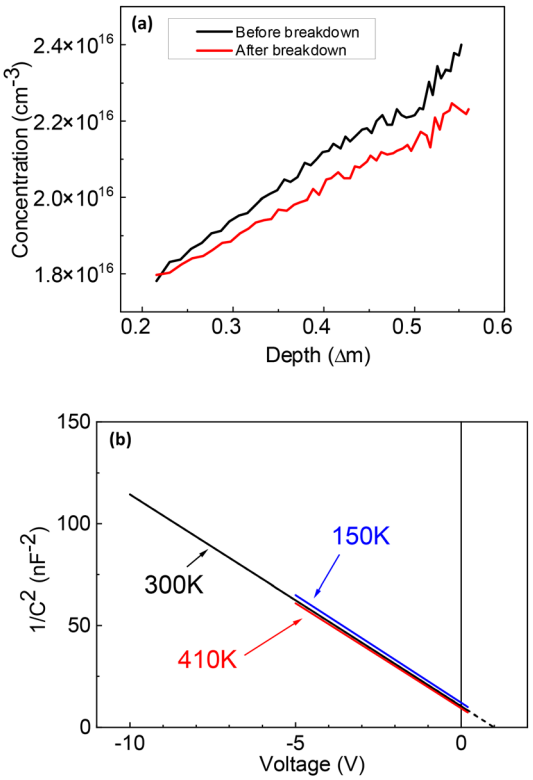

Fig. 3 (a) Room temperature charge concentration profiles calculated from C–V measurements before breakdown (black line) and after breakdown (red line); (b) $1/C^2$ *versus* voltage plots for the 380 μm diameter diode at different temperatures.

limits the maximal current and prevents the irreversible catastrophic breakdown.) The breakdown voltage increases considerably as the diode diameter decreases. Specifically, the BV was 330 V for 200 μm diameter diode, 225 V for 300 μm diode, and 200 V for 380 μm diode. Such strong dependence of the breakdown voltage on diameter has been observed previously[20] and attributed to the presence of certain extended defects. Indeed, the existence of such defects can be inferred from EBIC mapping.

After such a soft breakdown, the samples were not irreparably damaged, but their reverse current increased considerably, as shown in Fig. 2(a). The temperature dependence of reverse current for such damaged diodes with diameter 380 μm is shown in Fig. 5(a). The reverse current was found to increase with voltage proportionally to $E^{1/2}$ (E being the electric field), which is the hallmark feature of the Poole–Frenkel current flow *via* hopping between the deep centers in the space charge region.[32] This leakage mechanism is described by the following equation:

$$I = CE\exp\left[\frac{-q\left(\varphi - \sqrt{\frac{qE}{\pi\varepsilon_s\varepsilon_0}}\right)}{k_B T}\right] \quad (1)$$

where C is a constant, E – electric field, q – elementary charge, ϕ – Poole–Frenkel emission potential barrier height, ε_s – the

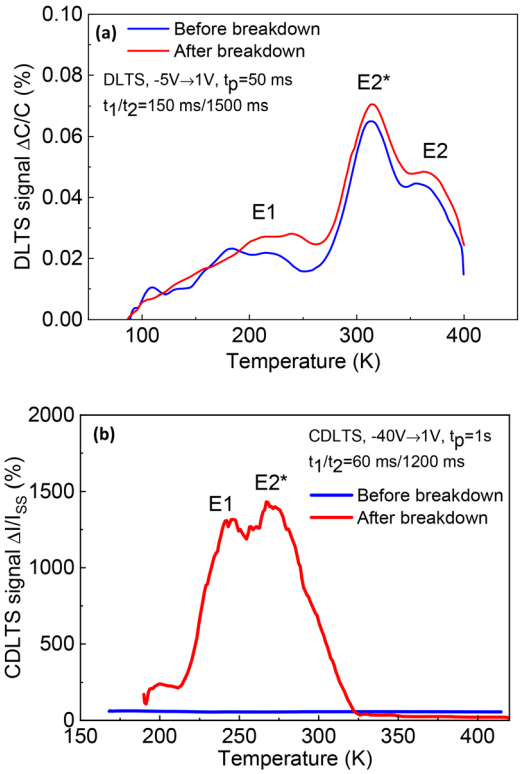

Fig. 4 (a) DLTS spectra measured for the 380 μm diameter diode before (blue line) and after (red line) breakdown, measurements were done with voltage pulsing from −5 V to 1 V (pulse length t_p = 50 ms), the spectra are shown for time windows 150 ms/1500 ms; (b) CDLTS spectra measured for the 380 μm diameter diode before (blue line) and after (red line) breakdown with reverse bias −40 V, forward pulsing to 1 V for 1 s, the signal ΔI is normalized by the steady-state current at −40 V, the spectra are shown for the time windows 60 ms/1200 ms.

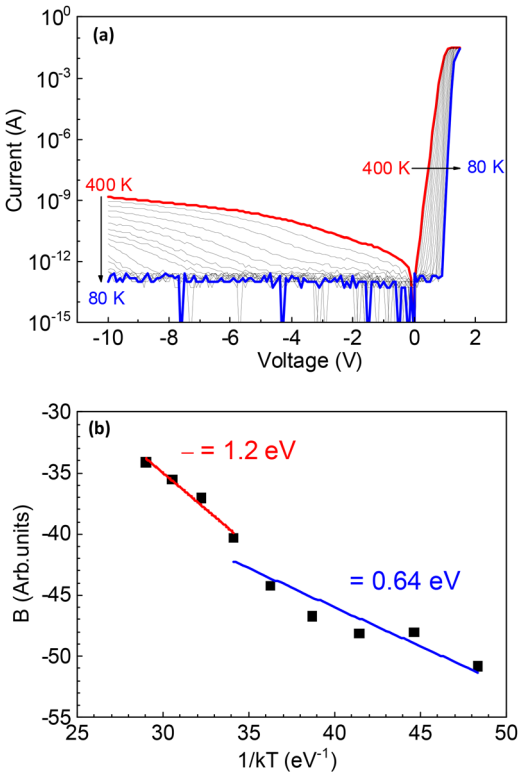

Fig. 5 (a) I–V characteristics measured at different temperatures after the breakdown for the 380 μm diameter diode; (b) the temperature dependence of coefficient B in Poole–Frenkel equation, used to calculate the height of the barrier ϕ.

relative dielectric constant, ε_0 – the permittivity of vacuum, k_B – Boltzmann constant, and T – temperature.

Then the current dependence on electric field is described by the expression (2):

$$\log\left(\frac{I}{E}\right) = A \bullet E^{1/2} + B \qquad (2)$$

where $A = \frac{q}{k_B T}\sqrt{\frac{q}{\pi\varepsilon_s\varepsilon_0}}$ is the curve slope, $B = \frac{-q\varphi}{k_B T} + \log C$ is the offset.

The temperature dependence of the B coefficient thus obtained is presented in Fig. 5(b). The dependence is not strictly linear, with the low temperature region showing the activation barrier 0.65 eV compatible with the energy of the dominant E2* center. Above room temperature the barrier is higher, 1.2 eV, possibly due to another deep center (possibly E3) not detected in our DLTS/CDLTS spectra.

The ideality factor in forward I–V characteristics became much higher than 1 at temperatures below 160 K, which is often attributed to the predominance of trap assisted tunneling (TAT) mechanism due to tunneling *via* deep traps,[31,46] presumably the dominant E2* centers[31] or possibly *via* E3 centers at higher temperatures. These observations suggest that the concentration of the said traps increases after the breakdown. However, the charge concentration profiles and DLTS spectra of such damaged samples are changed only slightly as can be seen from Fig. 3 and 4. In the CDLTS spectra in Fig. 4(b) one observes emergence of strong features due to the E2* and E1 traps not present in the pristine spectra. The explanation we propose is that the distribution of the centers is highly nonuniform and contributes to strong changes in the current flowing through regions with locally strongly enhanced concentration of deep traps. Note also that the Poole–Frenkel analysis also suggests the emergence of the E3 defect centers after the breakdown. These centers, however, are not clearly seen in CDLTS spectra because the reverse current at high voltages is too high at high temperatures necessary to detect this trap.

It should be mentioned that CDLTS spectra shown in Fig. 4(b) are depicted for time windows shorter than for DLTS spectra in Fig. 4(a) and for much higher quiescent reverse bias. The necessity to use shorter time windows comes from CDLTS sensitivity being lower than in DLTS. However, in contrast to DLTS, the signal in CDLTS increases in magnitude with shorter time window t_1 as $1/t_1$,[40] hence the use of shorter time windows, although even with the same time windows as used in DLTS we still see a measurable signal in CDLTS spectra, albeit with much lower magnitude.

EBIC mapping supports this explanation, as can be seen from Fig. 6 and 7. At 0 V bias we observe in diodes not subjected

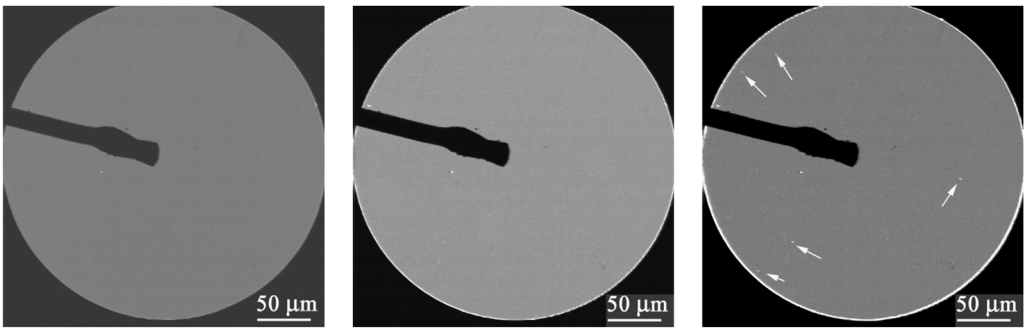

Fig. 6 EBIC maps of the 300 μm diode before the breakdown as obtained with different applied reverse voltage.

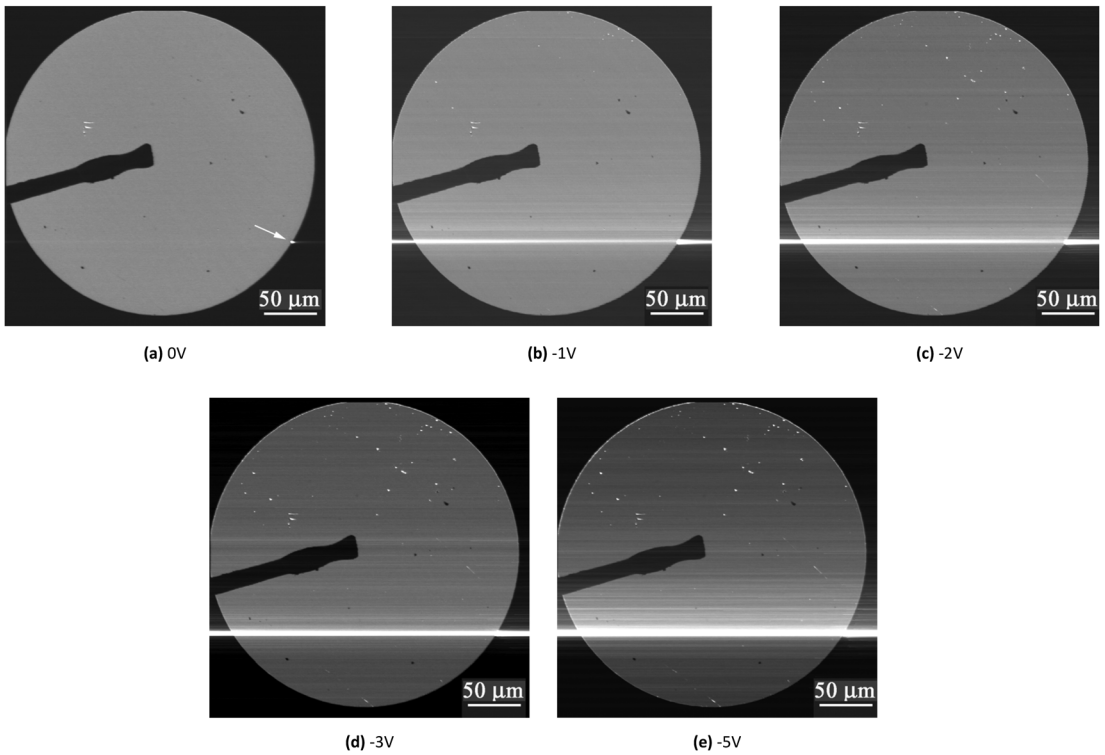

Fig. 7 EBIC maps of the 300 μm diode after breakdown for different applied reverse voltages.

to breakdown, that there are featureless images in EBIC mode (Fig. 6(a)). With increasing bias, bright contrast appears on the diode rim (Fig. 6(b)). At 5 V reverse bias, a few bright points can be also seen in the EBIC image (marked with arrows in Fig. 6(c)). In contrast, for the diodes after the soft breakdown, one bright spot can be seen even at 0 bias (marked with arrows in Fig. 7(a)). New bright dots inside the diode and horizontal lines appear already at 1 V with the brightest one associated with the defect seen at 0 V (Fig. 7(b)). With increasing bias, both bright dots and lines number and their brightness increases (Fig. 7(c–e)). Similar behavior has been already observed in κ-Ga_2O_3.[47] The bright dots in the EBIC mode are due to local enhancement of collected current, *i.e.* current gain. At the current high enough the amplifier is overloaded, and its relaxation leads to appearance of bright lines, with the width increasing with the local gain. Gain in the Schottky barriers increases with electric field.[47,48] Thus, the appearance of bright spots and increase of both their number and intensity shows that some extended defects or/and point defect agglomerates are present in the crystal, which enhance electric field near metal/Ga_2O_3 interface. After soft breakdown, the density of such defects increases.

Transmission electron microscope studies[27,28] indicate that, even in high-quality epilayers, defects, such strings of Ga vacancies and amorphized regions, are formed during electric breakdown and give rise to excessive leakage paths. Recently, conductive interstitial Ga-related line defects were observed in β-Ga_2O_3.[49] All such defects could increase local electric field

and hole trapping on them could lead to the local collected current gain, and in turn to the bright EBIC contrast. Recently, it has also been suggested that bunches of split Ga vacancies can be formed, which results in excess leakage.[50] Our CDLTS spectra measured after breakdown could point to generation of high densities of E1 and E2* centers in the vicinity of such agglomerates.

Another noteworthy fact that is that near the breakdown, repeated measurements of *I–V* characteristics show definite trends. Fig. 8 shows the *I–V* characteristics in one of the 200 μm diameter diodes measured after several sweeps bringing the voltage close to breakdown but not exceeding it. The shape of the *I–V* characteristics strongly implies that, at high voltages, the current flow is determined by the space-charge-limited current (SCLC).[24] The region of rapid increase of current with voltage of the form I–V^{α} with high α values shows a steady shift to higher threshold voltage values with each consecutive voltage sweep, presumably because of the increased thickness of the layer in which traps are filled after previous voltage sweeps.[24] When changing the direction of voltage sweep in this voltage region, one observes strong hysteresis of the *I–V* characteristics because of the changes of the filling of the traps. The effect is more pronounced after the soft breakdown. The width of the hysteresis reflects the change in the accumulated charge on the traps and is less pronounced at high temperatures.

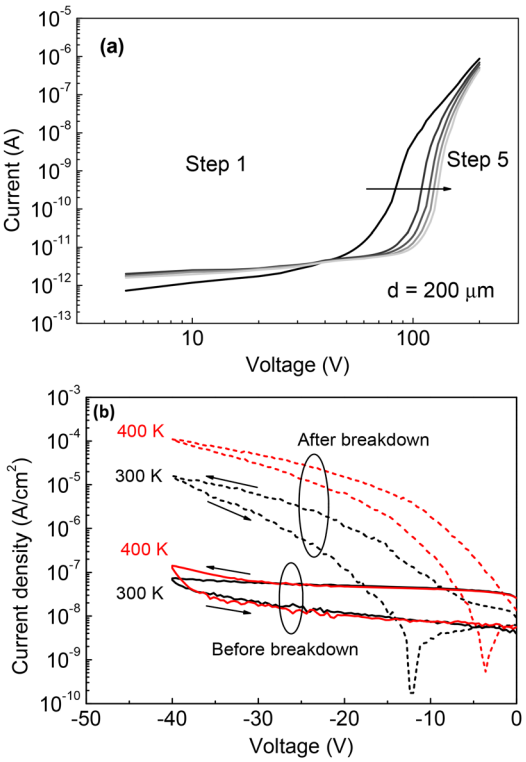

Fig. 8 (a) Current–voltage characteristics measured on 200 μm diameter diode in several consecutive tries; (b) reverse current hysteresis before (solid lines) and after (dashed lines) breakdown; measurements are shown for 300 K (black lines) and 400 K (red lines), the arrows indicate the direction of the voltage sweep.

As seen in Fig. 8(b) the integrated charge is much higher after the breakdown and the width of the loop decreases at elevated temperature (the data are presented for two sweep directions indicated by arrows and for two temperatures, 290 K (black lines) and 400 K (red lines)).

Conclusions

We have studied electrical properties and deep trap spectra before and after soft electric breakdown for different diameter Schottky diode rectifiers prepared on commercial n/n$^+$ Ga_2O_3 epistructures. Such structures show low reverse leakage current at room temperature, and the deep traps spectra in them are dominated by E2* centers (E_c −0.72 eV) associated with V_{Ga}–V_O. divacancies.[33] Two other deep traps detected were the E2 (E_c −0.8 eV) acceptors due to substitutional Fe on Ga site and the E1 (E_c −0.6 eV) acceptors attributed to Si–H complexes.[33] At high reverse voltage, the *I–V* characteristics are determined by the SCLC mechanism.[24] The soft breakdown voltage (*i.e.* breakdown mitigated by a high resistance in series with the source thus preventing the sample destruction) strongly increases with decreasing the diodes diameter in the order 330 V/225 V/200 V for diameters 200 μm/300 μm/380 μm, respectively. It could be mentioned that the breakdown can also justifiably be called as "soft" in the sense assigned to the term in ref. 51 where it is called because the breakdown is to large extent caused by the changes induced in the Schottky barrier height but the deep centers. As we have seen above, that seems to be a plausible explanation of the observed phenomena. After the breakdown, the reverse current strongly increased and, at moderate reverse voltages, was determined by Poole–Frenkel type hopping *via* deep traps in which the E2* traps played a prominent role. This would suggest a strong increase in density of the deep traps participating in hopping. However, the increase in capacitance DLTS and changes in concentration profiles calculated from *C–V* measurements were small. However, in current DLTS, a strong signal due to the E1, E2* traps emerged, suggesting that the traps determining the current increase are located near extended defects created (or transformed) at high reverse voltages. EBIC mapping of the samples after the breakdown indicates the appearance of extended defects giving rise to enhanced leakage. The presence of such defects explains the dependence of the breakdown voltage on the diodes area.[52,53] The role of different deep traps in premature breakdown of Ga_2O_3 Schottky diodes shows these being the E2*(E_c −0.76 eV),[31] E3 (E_c −1.1 eV),[36] E1-like E_c −0.46 eV[30] centers. The E3 centers have not been detected in the Schottky diodes in the present work. The E2* and E1 centers concentrations increased judging by CDLTS spectra measurements, but not in capacitance DLTS, which suggests that the density of these centers increases locally near some extended defects both inside the diodes and at the diodes boundaries where the electric field is strong. EBIC mapping reveals the presence of such defects emerging after the breakdown and serving as high leakage sites for increasing reverse voltage.

The exact atomic structure of these defects needs further investigation. In view of the results presented here, one might consider whether the different deep traps found to be correlated with the observed premature breakdown voltages are indeed the cause of these premature breakdowns or the markers indicating that the centers in question are segregated near the extended defects actually causing the premature breakdown.

Author contributions

A. Y. Polyakov: conceptualization, methodology, validation, investigation, writing, supervision. I. V. Shchemerov: methodology, validation, investigation, writing. E. B. Yakimov: methodology, validation, investigation, writing. A. V. Chernykh: methodology, writing. S. V. Chernykh: methodology, writing. A. A. Vasilev: methodology, writing. N. R. Matros: methodology, validation. A. A. Romanov: methodology, validation. L. A. Alexanyan: methodology, validation. E. E. Yakimov: methodology, validation, investigation, writing. S. J. Pearton: methodology, validation, investigation, writing.

Conflicts of interest

There are no conflicts to declare.

Data availability

Data for this article are available within the text.

Acknowledgements

The work at NUST MISIS was supported initially by a grant from the Ministry of Science and Higher Education of Russian Federation (Agreement No. 075-15-2022-1113) and then by a grant from the Russian Science Foundation (Agreement 25-72-10020). The work at IMT RAS was supported by the State Task No 075-00295-25-00. The work at UF was performed as part of the Interaction of Ionizing Radiation with Matter University Research Alliance (IIRM-URA), sponsored by the Department of the Defense, Defense Threat Reduction Agency, under Award No. HDTRA1-20-2-0002, monitored by Jacob Calkins.

References

1 *Gallium Oxide: Materials Properties, Crystal Growth, and Devices*, ed. M. Higashiwaki and S. Fujita, Springer Series in Materials Science, 2021, DOI: 10.1007/978-3-030-37153-1.
2 K. Sasaki, Prospects for β-Ga_2O_3: now and into the future, *Appl. Phys. Express*, 2024, **17**, 090101, DOI: 10.35848/1882-0786/ad6b73.
3 J.-S. Li, H.-H. Wan, C.-C. Chiang, T. J. Yoo, M.-H. Yu, F. Ren, H. Kim, Y.-T. Liao and S. J. Pearton, Breakdown up to 13.5 kV in NiO/β-Ga_2O_3 Vertical Heterojunction Rectifiers, *ECS J. Solid State Sci. Technol.*, 2024, **13**, 035003.
4 *Ultrawide Bandgap β-Ga_2O_3 Semiconductor: Theory and Applications, ed J. S. Speck and E. Farzana,* AIP Publishing, Melville, New York, 2023.
5 H. Peelaers, J. L. Lyons, J. B. Varley and C. G. Van de Walle, Deep acceptors and their diffusion in Ga_2O_3, *APL Mater.*, 2019, **7**, 022519, DOI: 10.1063/1.5063807.
6 X. Lu, Y. Deng, Y. Pei, Z. Chen and G. Wang, Recent advances in NiO/Ga_2O_3 heterojunctions for power electronics, *J. Semicon.*, 2023, **44**, 061802.
7 M. M. Islam, M. O. Liedke, D. Winarski, M. Butterling, A. Wagner, P. Hosemann, Y. Q. Wang, B. Uberuaga and F. Selim, A, Chemical manipulation of hydrogen induced high p-type and n-type conductivity in Ga_2O_3, *Sci. Rep.*, 2020, **10**(1), 6134.
8 E. Chikoidze, A. Fellous, A. Perez-Tomas, G. Sauthier,T. Tchelidze, C. Ton-That, T. Thanh Huynh, M. Phillips, S. Russell, M. Jennings, B. Berini, F. Jomard and Y. Dumont, P-type β-gallium oxide: A new perspective for power and optoelectronic devices, *Mater. Today Phys.*, 2017, **3**, 118e126.
9 E. Chikoidze, C. Sartel, H. Yamano, Z. Chi, G. Bouchez, F. Jomard, V. Sallet, G. Guillot, K. Boukheddaden, A. Pérez-Tomás, T. Tchelidze and Y. Dumont, Electrical properties of p-type Zn:Ga_2O_3 thin films, *J. Vac. Sci. Technol. A*, 2022, **40**, 043401, DOI: 10.1116/6.0001766.
10 Y. Lu, L. Jia, D. Chen, T. Li, H. Qi, X. Xu, X. Li, M. Zhu, H. Zhang and X. Lu, Insight into the High Hole Concentration of p-Type Ga_2O3 via In Situ Nitrogen Doping, *J. Phys. Chem. Lett.*, 2025, **16**, 4243, DOI: 10.1021/acs.jpclett.5c00318.
11 E. Chikoidze, C. Sartel, H. Mohamed, I. Madaci, T. Tchelidze, M. Modreanu, P. Vales-Castro, C. Rubio, C. Arnold, V. Sallet, Y. Dumont and A. Perez-Tomas, Enhancing the intrinsic p-type conductivity of the ultra-wide bandgap Ga_2O_3 semiconductor, *J. Mater. Chem. C*, 2019, **7**, 10231–10239, DOI: 10.1039/C9TC02910A.
12 C. E. Dreyer, A. Janotti, J. L. Lyons and D. Wickramaratne, Defects in semiconductors, Special Collection: Defects in Semiconductors 2024, *J. Appl. Phys.*, 2024, **136**, 190401, DOI: 10.1063/5.0244142.
13 P. Deak, Q. Duy Ho, F. Seemann, B. Aradi, M. Lorke and T. Frauenheim, Choosing the correct hybrid for defect calculations: A case study on intrinsic carrier trapping in β-Ga_2O_3, *Phys. Rev. B*, 2017, **95**, 075208, DOI: 10.1103/PhysRevB.95.075208.
14 M. E. Ingebrigtsen, A. Yu Kuznetsov, B. G. Svensson, G. Alfieri, A. Mihaila, U. Badstübner, A. Perron, L. Vines and J. B. Varley, Impact of proton irradiation on conductivity and deep level defects in β-Ga_2O_3, *APL Mater.*, 2019, **7**, 022510, DOI: 10.1063/1.5054826.
15 Y. Knausgård Hommedal, M. Etzelmüller Bathen, V. Mari Reinertsen, K. Magnus Johansen, L. Vines and Y. Kalmann Frodason, Theoretical modeling of defect diffusion in wide bandgap semiconductors, *J. Appl. Phys.*, 2024, **135**, 170902, DOI: 10.1063/5.0205866.
16 J. Kim, S. J. Pearton, C. Fares, J. Yang, F. Ren, S. Kima and A. Y. Polyakov, Radiation damage effects in Ga_2O_3 materials and devices, *J. Mater. Chem. C*, 2019, **7**, 10.

17 S. J. Pearton, F. Ren, A. Y. Polyakov, E. B. Yakimov, L. Chernyak and A. Haque, Perspective on comparative radiation hardness of Ga_2O_3 Polymorphs, *J. Vac. Sci. Technol. A*, 2025, **43**, 038501, DOI: **10.1116/6.0004444**.

18 Z. Zhang, E. Farzana, A. R. Arehart and S. A. Ringel, Deep level defects throughout the bandgap of (010) β-Ga_2O_3 detected by optically and thermally stimulated defect spectroscopy, *Appl. Phys. Lett.*, 2016, **108**, 052105.

19 A. Y. Polyakov, V. I. Nikolaev, E. B. Yakimov, F. Ren, S. J. Pearton and J. Kim, Deep level defect states in β-, α-, and ε-Ga2O3 crystals and films: Impact on device performance, *J. Vac. Sci. Technol. A*, 2022, **40**, 020804, DOI: **10.1116/6.0001701**.

20 J. Zhang, P. Dong, K. Dang, Y. Zhang, Q. Yan, H. Xiang, J. Su, Z. Liu, M. Si, J. Gao, M. Kong, H. Zhou and Y. Hao, Ultra-wide bandgap semiconductor Ga_2O_3 power Diodes, *Nat. Commun.*, 2022, **13**, 3900, DOI: **10.1038/s41467-022-31664-y**.

21 J. S. Li, C. C. Chiang, H. H. Wan, F. Ren and S. J. Pearton, Reproducibility of 10 kV-class NiO/Ga_2O_3 heterojunction rectifiers, *Appl. Phys. A: Mater. Sci. Process.*, 2025, **131**, 431, DOI: **10.1007/s00339-025-08527-6**.

22 F. Zhou, H. Gong, M. Xiao, Y. Ma, Z. Wang, X. Yu, L. Li, L. Fu, H. H. Tan, Y. Yang, F. F. Ren, S. Gu, Y. Zheng, H. Lu, R. Zhang, Y. Zhang and J. Ye, An avalanche-and-surge robust ultrawide-bandgap heterojunction for power electronics, *Nat. Commun.*, 2023, **14**, 4459.

23 H. Liu, Y. Wang, Y. Lv, S. Han, T. Han, S. Dun, H. Guo, A. Bu and Z. Feng, 10-kV lateral β-Ga_2O_3 MESFETs with B ion implanted planar isolation, *IEEE Electron Device Lett.*, 2023, **44**, 1048–1051.

24 X. Yu, H. Gong, J. Zhou, Z. Shen, W. Xu, T. You, J. Wang, S. Zhang, Y. Wang, K. Zhang, R. Tao, Y. Wu, F.-F. Ren, X. Ou, Y. Kong, Z. Li, T. Chen, D. Chen, S. Gu, Y. Zheng, J. Ye and R. Zhang, High-voltage β-Ga_2O_3 RF MOSFETs with a shallowly-implanted 2DEG-like channel, *IEEE Electron Device Lett.*, 2023, **44**, 1060–1063.

25 R. Zhang and Y. Zhang, Power device breakdown mechanism and characterization:Review and perspective, *Jpn. J. Appl. Phys*, 2023, **62**, Sc0806.

26 N. Daram Ramdin, H.-L. Huang, C. Chae, S. Dhara, S. Rajan, J. Hwang and L. J. Brillson, Impact of metal diffusion, lattice distortions, native defects, and ambient on dielectric breakdown in Ni–Ga_2O_3 Schottky diodes, *APL Mater.*, 2024, **12**(10), 101118, DOI: **10.1063/5.0228825**.

27 Z. Islam, A. Haque, N. Glavin, M. Xian, F. Ren, A. Y. Polyakov, A. Kochkova, M. Tadjer and S. J. Pearton, In Situ Transmission Electron Microscopy Observations of Forward Bias Degradation of Vertical Geometry β-Ga_2O_3 Rectifiers, *ECS J. Solid State Sci. Technol.*, 2020, **9**, 055008, DOI: **10.1149/2162-8777/ab981d**.

28 N. Sultan Al-Mamun, J.-S. Li, A. Haque, D. E. Wolfe, F. Ren and S. Pearton, High temperature operation and failure of Ga2O3 Schottky barrier diodes: An in situ TEM study, *APL Electron. Dev.*, 2025, **1**(1), 016103, DOI: **10.1063/5.0250729**.

29 Z. Islam, M. Xian, A. Haque, F. Ren, M. Tadjer, N. Glavin and S. Pearton, In situ observation of β-Ga_2O_3 Schottky diode failure under forward biasing condition, *IEEE Trans. Electron Devices*, 2020, **67**(8), 3056–3061, DOI: **10.1109/ted.2020.3000441**.

30 M. S. Haseman, D. N. Ramdin, W. Li, K. Nomoto, D. Jena, H. Grace Xing and L. J. Brillson, Electric field induced migration of native point defects in Ga_2O_3 devices, *J. Appl. Phys.*, 2023, **133**, 035701, DOI: **10.1063/5.0124543**.

31 H. Gong, X. Yang, M. Porter, Z. Yang, B. Wang, L. Li, L. Fu, K. Sasaki, H. Wang, S. Gu, R. Zhang, J. Ye and Y. Zhang, Reliability of NiO/β-Ga_2O_3 bipolar heterojunction, *Appl. Phys. Lett.*, 2025, **126**, 012102, DOI: **10.1063/5.0243015**.

32 S. Bu, Y. Wang, X. Zheng, S. Yue, D. Lin, L. Yi, V. Melikyan, X. Ma and Y. Hao, Forward bias stress-induced degradation mechanism in β-Ga_2O_3 SBDs: A trap-centric perspective, *Appl. Phys. Lett.*, 2025, **126**, 122104, DOI: **10.1063/5.0260529**.

33 M. E. Levinshtein, S. L. Rumyantsev and M. Shur, *Properties of Advanced Semiconductor Materials GaN, AlN, InN, BN, SiC, SiGe*, John Wiley, New York, 2001.

34 A. Langørgen, L. Vines and Y. Kalmann Frodason, Perspective on electrically active defects in β-Ga_2O_3 from deep-level transient spectroscopy and first-principles calculations, *J. Appl. Phys.*, 2024, **135**, 195702, DOI: **10.1063/5.0205950**.

35 Y. Zhang, J. Zhang, H. Zhou, T. Zhang, H. Wang, Z. Feng and Y. Hao, *Solid-State Electron.*, 2020, **169**(10), 107807, DOI: **10.1016/j.sse.2020.107807**.

36 M. Xian, R. Elhassani, C. Fares, F. Ren, M. Tadjer and S. J. Pearton, Forward bias degradation and thermal simulations of vertical geometry β-Ga_2O_3 Schottky rectifiers, *J. Vac. Sci. Technol. B*, 2019, **37**(6), 061205, DOI: **10.1116/1.5127511**.

37 K. Egbo, W. A. Callahan, S. Sohel, C. Chae, B. Tellekamp, J. Hwang and A. Zakutayev, Thermally induced PtO_x interfacial layer enhances stability of Pt/β-Ga_2O_3 vertical Schottky diodes, *APL Energy*, 2025, **3**(1), 016104, DOI: **10.1063/5.0251435**.

38 Y. Wang, X. Zheng, J. Zhu, A. Pan, S. Bu, Y. Hong, J. Zhang, L. Guo, X. Ma and Y. Hao, On-state electrical stress-induced degradation of NiO/β-Ga_2O_3 heterojunction pn diodes, *Appl. Phys. Lett.*, 2024, **124**, 193503, DOI: **10.1063/5.0204051**.

39 Z. P. Wang, N. Sun, X. X. Yu, H. H. Gong, X. L. Ji, F.-F. Ren, S. L. Gu, Y. D. Zheng, R. Zhang, A. Y. Kuznetsov and J. D. Ye, On-state electrical stress-induced degradation of NiO/β-Ga2O3 heterojunction pn diodes, Performance limiting inhomogeneities of defect states in ampere-class Ga_2O_3 power diodes, *Appl. Phys. Rev.*, 2024, **11**, 021413, DOI: **10.1063/5.0191343**.

40 D. K. Schroder, *Semiconductor material and device characterization*, Wiley&Sons, Inc., New York, 1990, p. 587.

41 A. Y. Polyakov, V. I. Nikolaev, S. I. Stepanov, A. I. Pechnikov, E. B. Yakimov, N. B. Smirnov, I. V. Shchemerov, A. A. Vasilev, A. I. Kochkova, A. V. Chernykh and S. J. Pearton, Editors' Choice—Electrical Properties and Deep Traps in α-Ga_2O_3:Sn Films Grown on Sapphire by Halide Vapor Phase Epitaxy, *ECS J. Solid State Sci. Technol.*, 2020, **9**, 045003.

42 A. Y. Polyakov, N. B. Smirnov, I.-H. Lee and S. J. Pearton, Deep level transient spectroscopy in III-Nitrides: decreasing the effects of series resistance, *J. Vac. Sci. Technol. B*, 2015, **33**, 061203.

43 A. Y. Polyakov, N. B. Smirnov, I. V. Shchemerov, S. J. Pearton, F. Ren, A. V. Chernykh, P. B. Lagov and T. V. Kulevoy, Hole traps and persistent photocapacitance in proton irradiated -Ga_2O_3 films doped with, *APL Mater.*, 2018, **6**, 096102, DOI: **10.1063/1.5042646**.

44 E. B. Yakimov, A. Y. Polyakov, N. B. Smirnov, I. V. Shchemerov, P. S. Vergeles, E. E. Yakimov, A. V. Chernykh, M. Xian, F. Ren and S. J. Pearton, Role of hole trapping by deep acceptors in electron-beam-induced current measurements in β-Ga_2O_3 vertical rectifiers, *J. Phys. D: Appl. Phys.*, 2020, **53**, 495108.

45 E. B. Yakimov, A. Y. Polyakov, I. V. Shchemerov, N. B. Smirnov, A. A. Vasilev, A. I. Kochkova, P. S. Vergeles, E. E. Yakimov, A. V. Chernykh, M. Xian, F. Ren and S. J. Pearton, On the nature of photosensitivity gain in Ga_2O_3 Schottky diode detectors: Effects of hole trapping by deep acceptors, *J. Alloys Compds*, 2021, **879**, 160394.

46 M. Mandurrino, M. Goano, M. Vallone, F. Bertazzi, G. Ghione, G. Verzellesi, M. Meneghini, G. Meneghesso and E. Zanoni, Semiclassical simulation of trap-assisted tunneling in GaN-based light-emitting diodes, *J. Comput. Electron.*, 2015, **14**, 444–455, DOI: **10.1007/s10825-015-0675-3**.

47 E. B. Yakimov, V. I. Nikolaev, A. I. Pechnikov, A. Y. Polyakov, I. V. Shchemerov, A. A. Vasilev, Y. O. Kulanchikov, P. S. Vergeles, E. E. Yakimov and S. J. Pearton, Electron Beam Induced Current Study of Photocurrent Gain in κ-Ga_2O_3 Schottky Diodes, *ECS J. Solid State Sci. Technol.*, 2023, **12**, 044009.

48 O. Katz, V. Garber, B. Meyler, G. Bahir and J. Salzman, Gain mechanism in GaN Schottky ultraviolet detectors, *Appl. Phys. Lett.*, 2001, **79**, 1417–1419.

49 A. Y. Polyakov, E. B. Yakimov, I. V. Shchemerov, A. A. Vasilev, A. I. Kochkova and V. I. Nikolaev, S J Pearton. Huge photosensitivity gain combined with long photocurrent decay times in various polymorphs of Ga_2O_3: effects of carrier trapping with deep centers, *J. Phys. D: Appl. Phys.*, 2025, **58**, 063002.

50 L. Wang, S. Liu, Z. Liu, M. Han, J. Tian, Y. Xiao, Q. Chen, D. Hu, L. Zhang, L. Kang and Q. Dai, Observation of Conductive Interstitial Ga Line Defects in β-Ga_2O_3, *Adv. Mater.*, 2025, **37**, 2418230, DOI: **10.1002/adma.202418230**.

51 T. Sugiura and N. Nakano, Hard- and Soft-Breakdown Modeling in ⟨001⟩ Oriented β-Ga2O3 Schottky barrier diode, *J. Appl. Phys.*, 2022, **132**, 175703, DOI: **10.1063/5.0125609)**.

52 J. S. Li, H. H. Wan, C. C. Chiang, T. J. Yoo, M. H. Yu, F. Ren, H. Kim, Y. T. Liao and S. J. Pearton, Breakdown up to 13.5 kV in NiO/β-Ga_2O_3 Vertical Heterojunction Rectifiers, *ECS J. Solid State Sci. Technol.*, 2024, **13**, 035003.

53 S. J. Pearton, F. Ren, A. Y. Polyakov, A. Haque, M. Labed and Y. S. Rim, Status of Ga_2O_3 for power device and UV photodetector applications, *Appl. Phys. Rev.*, 2025, **12**, 031336.